Mechanism of Metal Doping in Regulating Boron Adsorption Performance of Fe_3O_4 Nanoparticles

Yumeng Jiang,[ab] Anni Yang,[cd] Huiqun Ju,[ab] Tianyu Li,[ab] Jiafei Lyu*[cd] and Xianghai Guo*[abc]

[a] *Tianjin Key Laboratory for Marine Environmental Research and Service, School of Marine Science and Technology, Tianjin University, Tianjin 300072, China*

[b] *Key Laboratory of Ocean Observation Technology of Ministry of Natural Resources, School of Marine Science and Technology, Tianjin University, Tianjin 300072, P. R. China*

[c] *Department of Pharmaceutical Engineering, School of Chemical Engineering and Technology, Tianjin University, Tianjin 300350, P. R. China*

[d] *Key Laboratory of Systems Bioengineering (Ministry of Education), Tianjin University, Tianjin, 300072, P. R. China*

* Corresponding author

Xianghai Guo, Email: guoxh@tju.edu.cn

Jiafei Lyu, Email: jflv@tju.edu.cn

Contents

1. Experiments

1.1 Raw Materials

All chemicals and solvents were purchased from commercial suppliers and used without further purification including ferric chloride hexahydrate ($FeCl_3 \cdot 6H_2O$, 99%, Aladdin, Shanghai, China), ferrous chloride tetrahydrate ($FeCl_2 \cdot 4H_2O$, 98%, Meryer, Shanghai, China), tetramethylammonium hydroxide ($N^+(CH_3)_4OH^-$, 25%w/w in water, Meryer, Shanghai, China), calcium chloride dihydrate ($CaCl_2 \cdot 2H_2O$, Meryer, Shanghai, China), magnesium chloride ($MgCl_2$, Meryer, Shanghai, China), zinc chloride ($ZnCl_2$, Meryer, Shanghai, China), chromic chloride ($CrCl_2$, Aladdin, Shanghai, China), copper chloride dihydrate ($CuCl_2 \cdot 2H_2O$, Meryer, Shanghai, China), cobalt chloride ($CoCl_2$, 99.7%, Macklin, Shanghai, China), manganese chloride ($MnCl_2$, Meryer, Shanghai, China), hydrochloric acid (36~38%, Yuanli, Tianjin, China), Mannitol ($C_6H_{14}O_6$, Aladdin, Shanghai, China), sodium hydroxide standard solution (NaOH, Aladdin, Shanghai, China), Deionized water was used as water source throughout the experiments.

1.2 Preparation of Fe_3O_4 magnetic nanoparticles

For magnetite nanoparticles synthesis, 1 M ferric chloride hexahydrate and 2 M ferrous chloride tetrahydrate were prepared by dissolving iron salts in 2 M HCl solutions, respectively. In a typical experimental procedure, 10 ml of 1 M $FeCl_3$ solution was mixed with 2.5 mL of 2 M $FeCl_2$ solution in a flask. Metal doped simples were synthesized via 10 ml of 1 M $FeCl_3$ 2.275 mL of 2 M $FeCl_2$ and 0.225 mL of 2 M MCl_2 (M=Ca, Mg, Zn, Cu, Co, Cr, Mn). This solution was stirred, followed by the slow addition of 21 mL 25% (w/w) $N^+(CH_3)_4OH^-$. The mixture was stirred for 25 minutes at a speed of 600 rpm using a magnetic heating stirrer. The doped samples were obtained by cationic substitution at 3% molar proportions in relation to Fe ions.

1.3 Characterization

X-ray diffraction (XRD) patterns of experimental sample were detected by Rigaku X-ray diffractometer (Smartlab SE) equipped with a rotating anode of 1.6 KW Cu-$K\alpha_1$

X-ray radiation (λ = 0.15406 nm). Measurements were made over the range of 10°＜ 2θ＜70° in a 0.05 step width with a 2°/min scanning speed. Scanning electron microscopy (SEM) images were obtained from ZEISS Sigma 360 operated at 3kV. Transmission electron microscope (TEM) images were obtained from JEOL JEM-2100F operated at 200kV. The magnetic characterization at room temperature was obtained using a vibrating sample magnetometer (VSM) Lakeshore 7404. X-ray photoelectron spectroscopy (XPS) was recorded by Thermo Scientific K-Alpha.

1.4 B analysis method

The boric acid concentration (Q_e) was obtained by acid-base titration. 1mL 0.5 M mannitol solution and two drops of 5% phenolphthalein indicator solution were added into a 50 mL conical bottle, and the mass M_1 was obtained (Sartorious BSA224S-CW). Then 0.2 mL of the post-adsorption solution was added and the mass M_2 was weighed. It was titrated with sodium hydroxide standard solution (0.05 mol /L) until pink, and the mass M_3 was obtained.

$$Q_e = \frac{M_3 - M_2}{M_2 - M_1} \times 0.05$$

1.5 Adsorption experiments

Before the adsorption studies, Fe_3O_4 magnetic nanoparticles was activated in a vacuum oven at 60 °C for 10 h. In a typical adsorption experiment, 0.05 g Fe_3O_4 or M@Fe_3O_4 (M= Ca^{2+}, Mg^{2+}, Zn^{2+}, Cu^{2+}, Co^{2+}, Mn^{2+}, Cr^{2+}) was added into a 50 mL centrifuge tube, followed by 10 mL boron aqueous solution with specific pH and concentration. The tube was placed in a thermostatic shaker at 45℃ for boron removal[1]. When the adsorption was completed, Fe_3O_4 or M@Fe_3O_4 was separated by magnetic field and the residual solution was examined for boron concentration.

1.6 Effect of *p*H on boron separation

The adsorption experiment was carried out with a series of boron solutions at pH=3-11. The *p*H was adjusted by 2 mol/L aqueous hydrochloric acid solution or 2 mol/L aqueous sodium hydroxide solution. The activated Mg@Fe_3O_4 was added to these prepared solutions with the dose of 5 $g \cdot L^{-1}$. The mixtures were placed in a

constant temperature shaker at 45 ℃ for 24 h. The adsorbent was separated by a magnet and the residual solutions were tested for boron concentration.

2. Figures

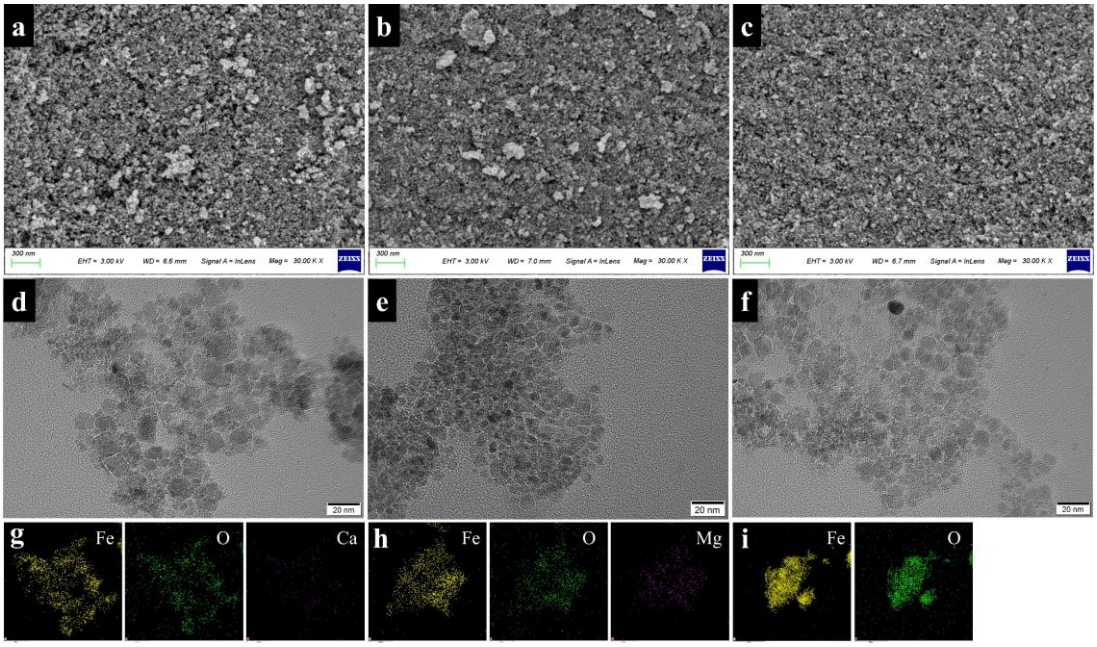

Fig. S1 SEM images of a) Ca@Fe_3O_4, b) Mg@Fe_3O_4, c) Fe_3O_4. TEM images of d) Ca@Fe_3O_4, e) Mg@Fe_3O_4, f) Fe_3O_4. TEM-EDS mapping of g) Ca@Fe_3O_4, h) Mg@Fe_3O_4, i) Fe_3O_4.

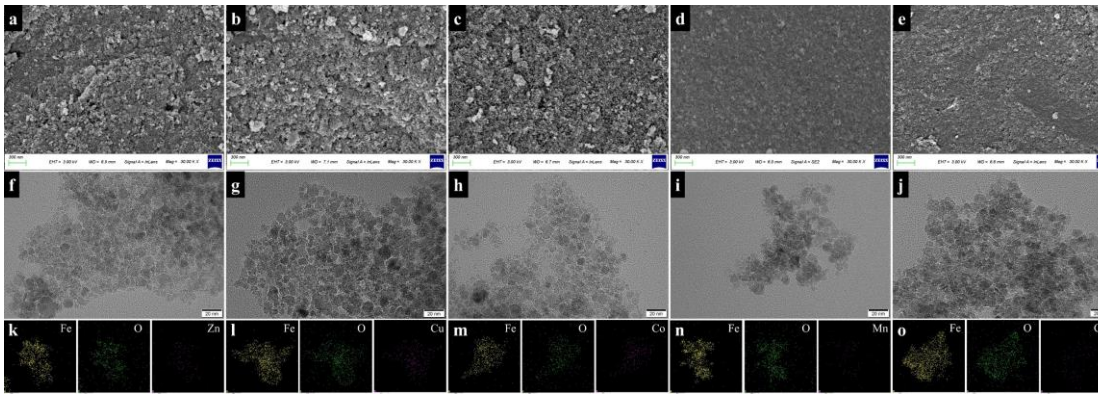

Fig. S2 SEM images of a) Zn@Fe_3O_4, b) Cu@Fe_3O_4, c) Co@Fe_3O_4, d) Mn@Fe_3O_4, e) Cr@Fe_3O_4. TEM images of f) Zn@Fe_3O_4, g) Cu@Fe_3O_4, h) Co@Fe_3O_4, i) Mn@Fe_3O_4, j) Cr@Fe_3O_4. TEM-EDS mapping of k) Zn@Fe_3O_4, l) Cu@Fe_3O_4, m) Co@Fe_3O_4, n) Mn@Fe_3O_4, o) Cr@Fe_3O_4.

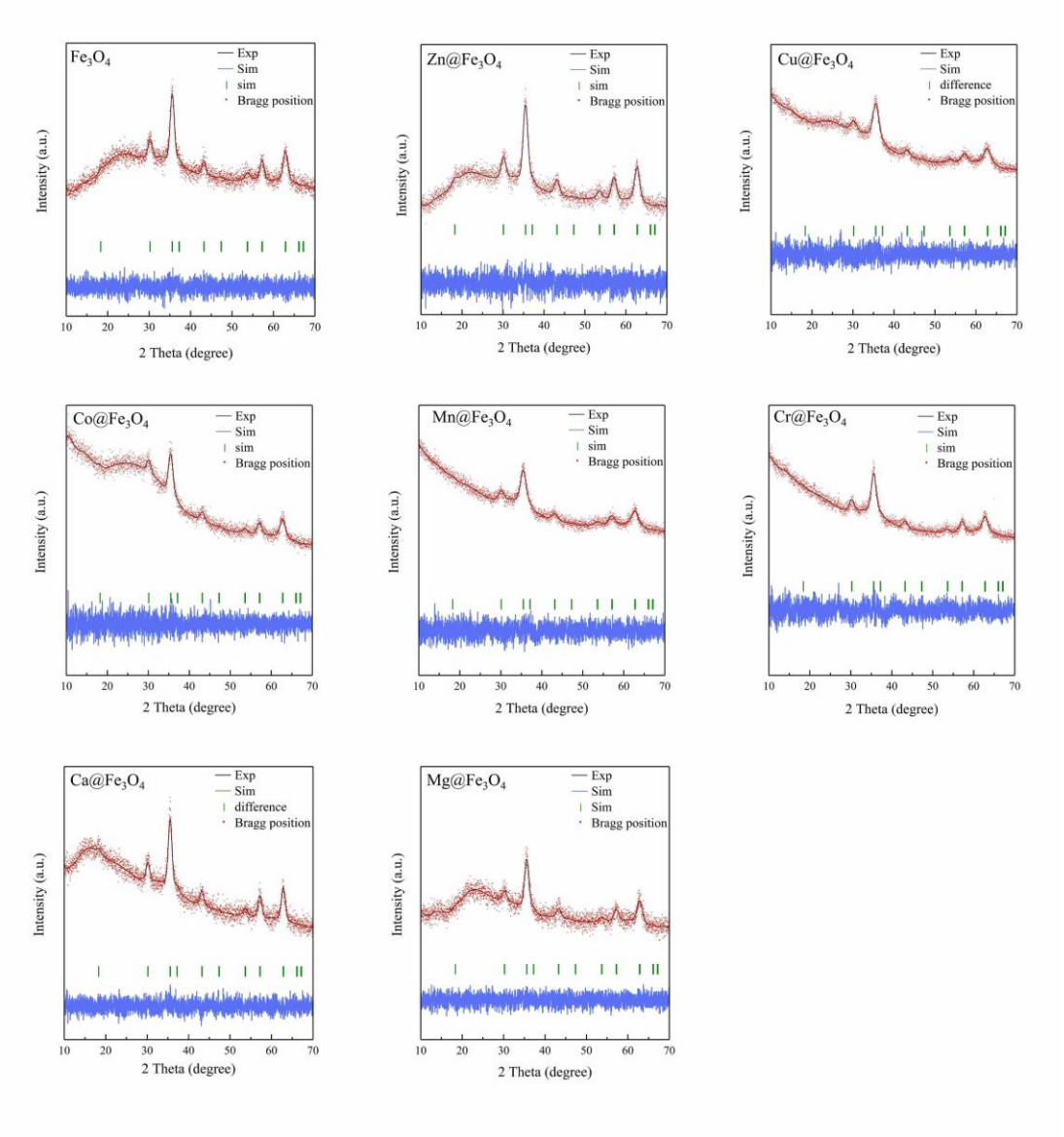

Fig. S3 Rietveld structural refinements for pristine and metal doped Fe_3O_4 materials.

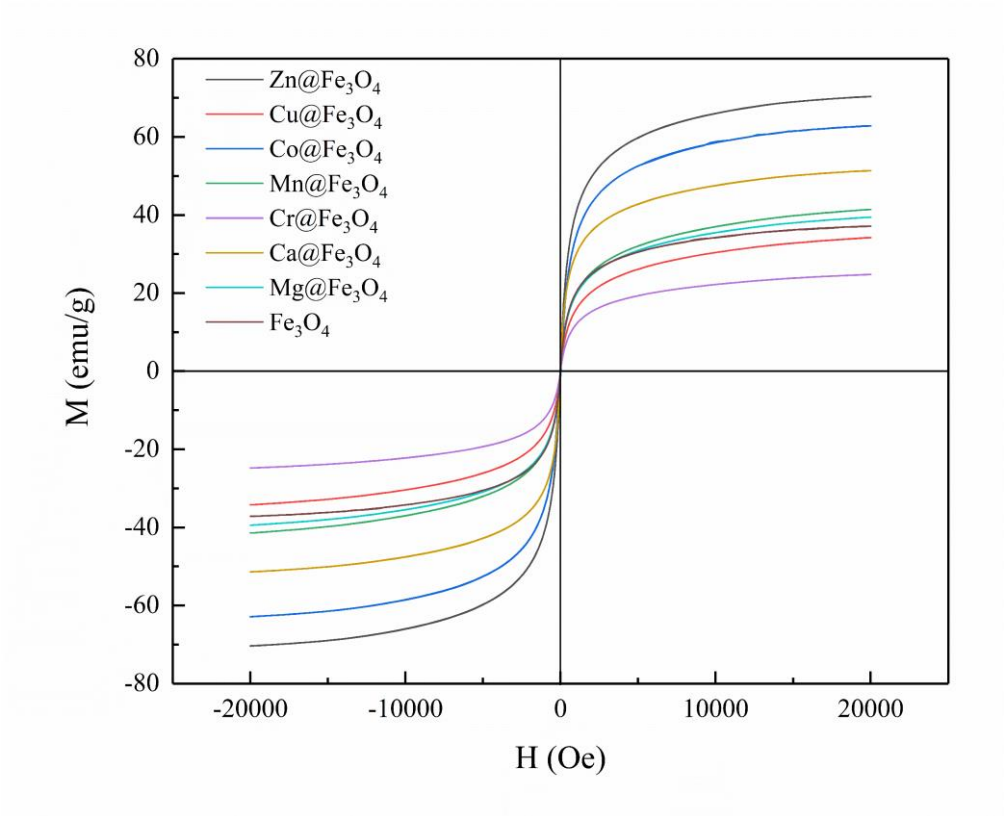

Fig. S4 The magnetic hysteresis loops of Fe_3O_4 and M@Fe_3O_4 powders.

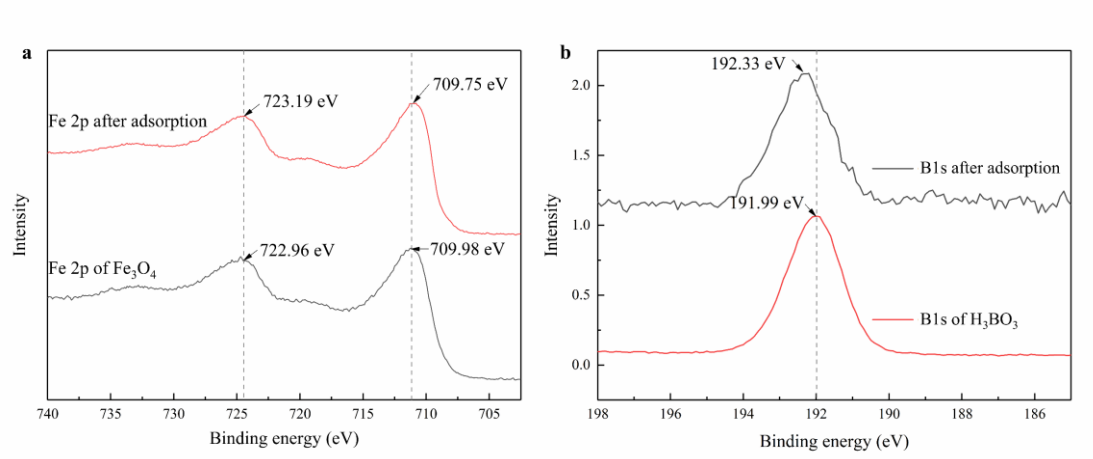

Fig. S5 XPS spectra of (a) Fe 2p before and after adsorption, (b) B1s of H_3BO_3 and after adsorption.

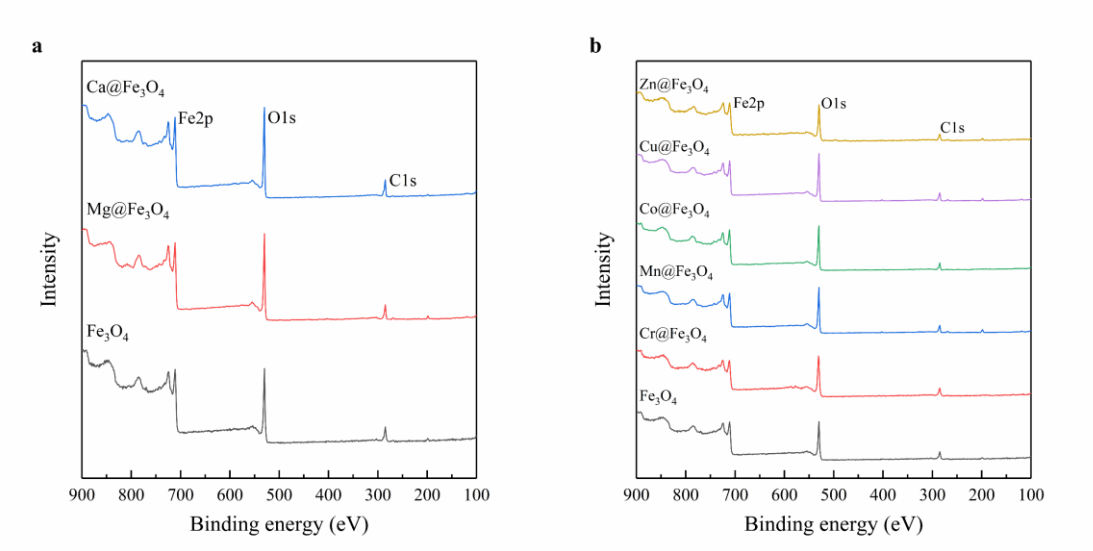

Fig. S6 (a) Comparison between XPS survey spectra for alkaline-earth metals doped Fe_3O_4 nanoparticles. (b) Comparison between XPS survey spectra for transition metals doped Fe_3O_4 nanoparticles.

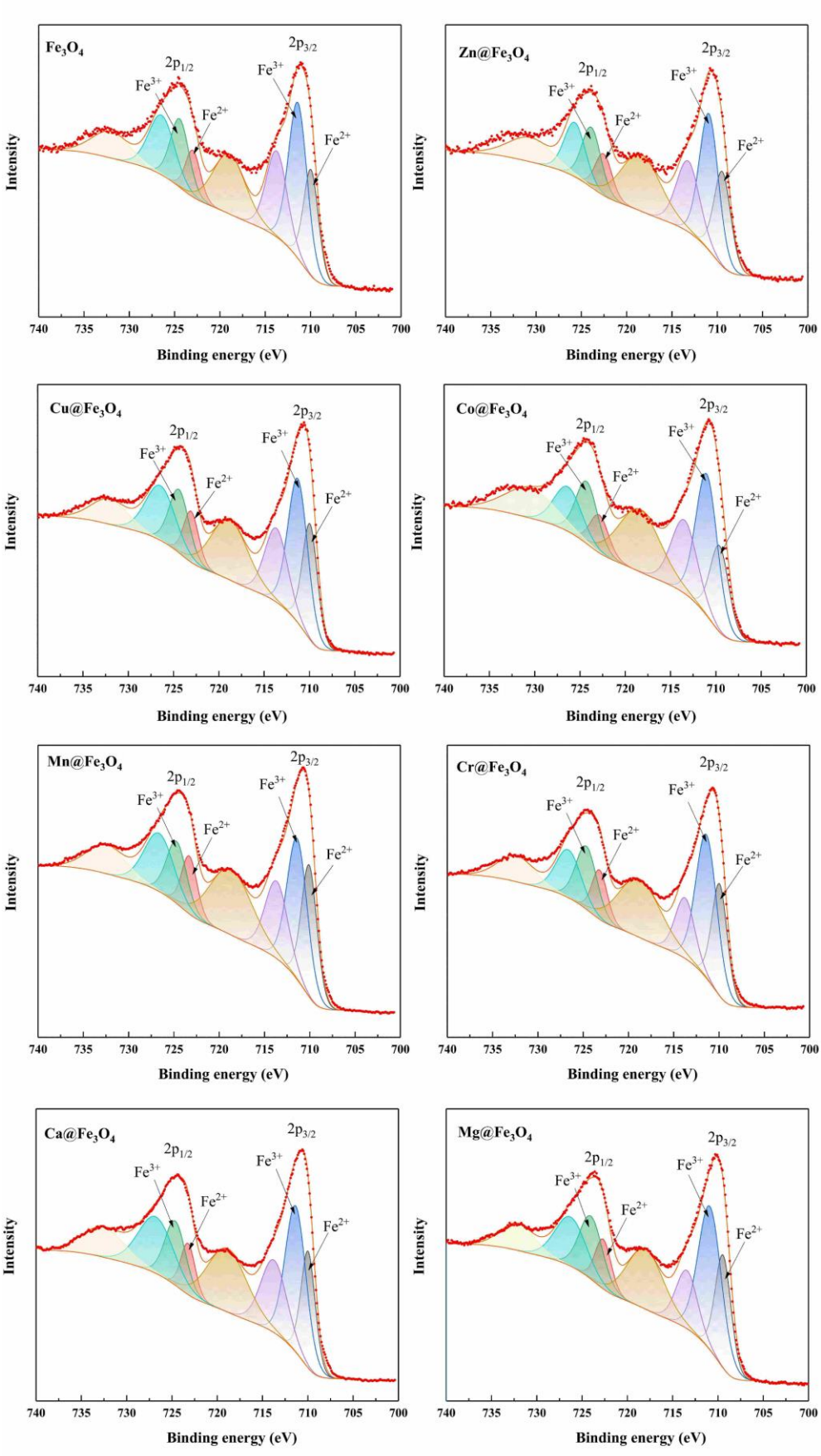

Fig. S7 XPS spectra of Fe 2p for Fe_3O_4 and M@Fe_3O_4 powders.

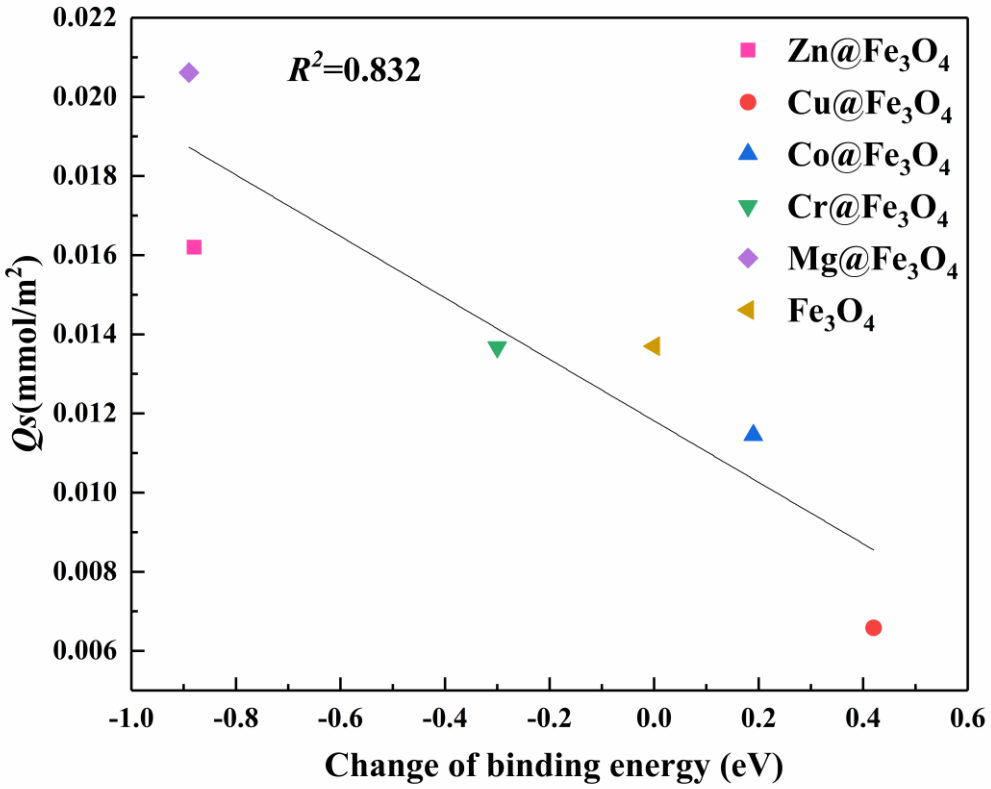

Fig. S8 The relationship between the shift in oxygen electron density in Fe-O-H of metals doped samples compared to pure Fe_3O_4 and boron adsorption capacity per unit area.

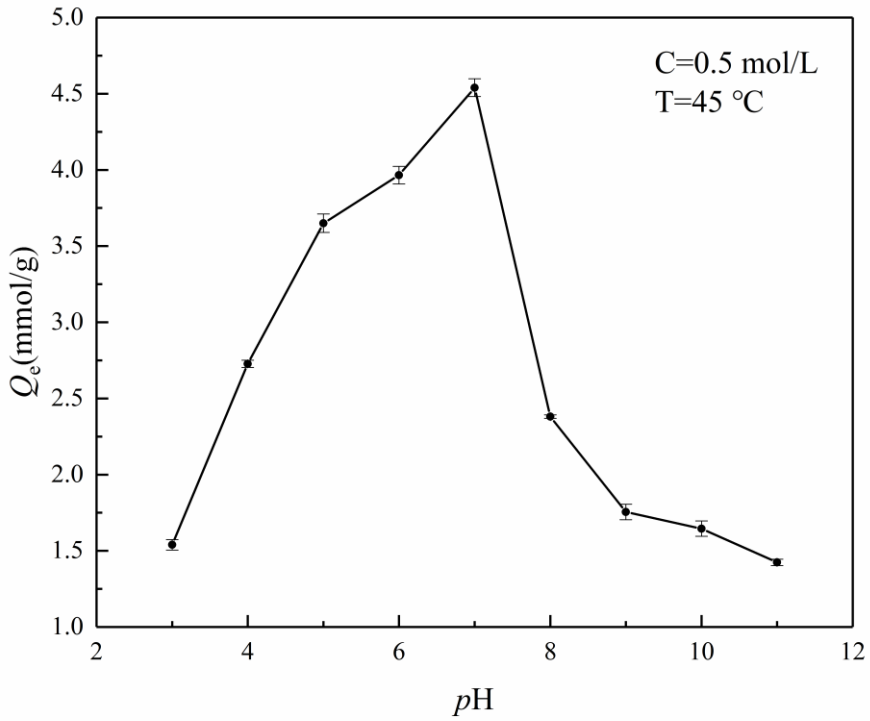

Fig. S9 Boron adsorption capacity on Mg@Fe_3O_4 at different *p*Hs.

3. Tables

Table S1 Ionic radius, electronegativity and electrode potential (M^{2+}/M) of doped metal and Fe^2

Metal	Ionic radius (pm)	Electronegativity (Pauling scale)	electrode potential (V)
Fe	76	1.83	−0.44
Zn	74	1.65	−0.76
Cu	72	1.90	0.34
Co	74	1.88	−0.28
Mn	80	1.55	−1.17
Cr	84	1.66	0.90
Ca	99	1.00	−2.84
Mg	65	1.31	−2.36

Table S2 FWHM and crystallite sizes of metal doped Fe3O4 nanoparticles

Samples	Actual doping percentage (%)	FWHM	Observed crystallite size (nm)	Calculated crystallite size (nm)
Fe_3O_4	−−	1.234°	7.0	6.7
$Zn@Fe_3O_4$	3.8	1.211°	8.0	6.9
$Cu@Fe_3O_4$	2.9	1.337°	7.5	6.3
$Co@Fe_3O_4$	3.2	1.261°	7.5	6.6
$Mn@Fe_3O_4$	2.7	1.175°	8.0	7.1
$Cr@Fe_3O_4$	3.0	1.140°	8.0	7.3
$Ca@Fe_3O_4$	2.2	0.801°	11.0	10.5
$Mg@Fe_3O_4$	3.3	1.301°	6.0	6.3

Table S3 Crystal structural parameters obtained by the Rietveld refinement

Samples	$a=b=c$ (Å)	R_{wp}%	R_p%	Space group
Fe_3O_4	8.354	2.03	1.62	Fd-3m
$Zn@Fe_3O_4$	8.365	1.96	1.55	Fd-3m
$Cu@Fe_3O_4$	8.365	4.14	3.28	Fd-3m
$Co@Fe_3O_4$	8.357	4.16	3.26	Fd-3m
$Mn@Fe_3O_4$	8.364	4.18	3.29	Fd-3m
$Cr@Fe_3O_4$	8.363	4.74	3.75	Fd-3m
$Ca@Fe_3O_4$	8.369	2.16	1.72	Fd-3m
$Mg@Fe_3O_4$	8.350	2.12	1.69	Fd-3m

Table S4 Magnetic and resistive parameters obtained for pure and doped Fe_3O_4 samples

Samples	Hc (G)	Mr (emu/g)	Ms (emu/g)
Fe_3O_4	0.4	0.03	37.11
$Zn@Fe_3O_4$	6.0	0.44	70.33
$Cu@Fe_3O_4$	0.65	0.03	34.18
$Co@Fe_3O_4$	22.8	1.52	62.79
$Mn@Fe_3O_4$	12.7	0.55	41.41
$Cr@Fe_3O_4$	0.6	0.02	24.76
$Ca@Fe_3O_4$	3.2	0.33	51.32
$Mg@Fe_3O_4$	0.5	0.03	39.42

Table S5 Fe2p binding energy in metal doped Fe_3O_4 nanoparticles

Samples	Fe^{2+} $2p_{3/2}$	Fe^{3+} $2p_{3/2}$	Fe^{2+} $2p_{1/2}$	Fe^{3+} $2p_{1/2}$	Fe^{3+}/ Fe^{2+}
Fe_3O_4	709.94	711.40	723.17	724.44	1.8
$Zn@Fe_3O_4$	709.89	711.61	723.15	724.60	1.8
$Cu@Fe_3O_4$	709.95	711.41	723.27	724.62	1.8
$Co@Fe_3O_4$	709.91	711.33	723.16	724.55	1.8
$Mn@Fe_3O_4$	709.90	711.36	723.25	724.68	1.8
$Cr@Fe_3O_4$	709.93	711.38	723.19	724.65	1.8
$Ca@Fe_3O_4$	709.97	711.34	723.18	724.64	1.8
$Mg@Fe_3O_4$	709.82	711.32	722.77	724.02	1.8

Table S6 Fe-O-Fe and Fe-O-H binding energy in metal doped Fe_3O_4 nanoparticles

Samples	Oxygen in Fe-O-Fe (eV)	Shift(eV)	Oxygen in Fe-O-H (eV)	Shift(eV)
Fe_3O_4	530.12	0	531.68	0
$Zn@Fe_3O_4$	529.91	−0.21	530.80	−0.88
$Cu@Fe_3O_4$	531.00	0.88	532.10	0.42
$Co@Fe_3O_4$	530.47	0.35	531.87	0.19
$Mn@Fe_3O_4$	529.82	−0.3	531.13	−0.55
$Cr@Fe_3O_4$	530.06	−0.06	531.38	−0.3
$Ca@Fe_3O_4$	529.26	−0.86	530.72	−0.96
$Mg@Fe_3O_4$	529.92	−0.2	530.79	−0.89

Table S7 Boron adsorption capacity for pure and doped Fe_3O_4 samples

Samples	*Qe* (mmol/g)	Specific surface area *A* (m^2/g)	*Qs* ($mmol/m^2$)
Fe_3O_4	2.36	173	0.0137
$Zn@Fe_3O_4$	2.72	168	0.0162
$Cu@Fe_3O_4$	1.21	184	0.0066
$Co@Fe_3O_4$	2.01	176	0.0115
$Mn@Fe_3O_4$	1.85	163	0.0113
$Cr@Fe_3O_4$	2.17	159	0.0137
$Ca@Fe_3O_4$	1.29	110	0.0117
$Mg@Fe_3O_4$	3.79	184	0.0206

Note: 1. Specific surface area *A* was evaluated by calculated crystallite sizes of nonporous spherical particle.

2. $Q_s = Q_e / A$

References:

1. T. Chen, Q. Wang, J. Lyu, P. Bai and X. Guo, *Separation and Purification Technology*, 2020, **231**, 1-10.
2. J. Speight, in *Lange's Handbook of Chemistry*, McGraw Hill LLC, McGraw Hill, September 2016, pp. 618-701.